ACS OMEGA

http://pubs.acs.org/journal/acsodf

Article

Research of the Collision Mechanics Model and Time-Frequency Characteristics during the Multistage Variable-Inclination Screening Process for Clean Coal

Long Huang,* Yuhan Liu, Jiawang Lu, Shijie Yu, Miao Pan, Jida Wu, Jinpeng Qiao, and Haishen Jiang*

Cite This: *ACS Omega* 2022, 7, 13963−13975

Read Online

ACCESS | Metrics & More | Article Recommendations

ABSTRACT: Equal-thickness screening is a critical part of mineral processing; recently, the multistage variable-inclination equal-thickness screen (MSVIETS) has been utilized in the mining industry across the world. In this work, a model of the collision mechanics between particles and the multistage variable-inclination screen surface was established. The maximum collision force (F_{max}) was found to be closely related to amplitude, frequency, screen surface inclination, and number of stages. The time-frequency response characteristics of multistage (3-, 4-, and 5-STAGE) screen surfaces were studied by the vibration test analysis system. The permeation screen distribution law of grain groups on the screen surface was revealed. The obtained results show the best screening performance can be obtained from the 5-STAGE scheme with a screening efficiency of higher than 95% and total mismatch content of less than 2%. The synergistic mechanism between two of the parameters was revealed by Box−Behnken response surface methodology (BBRSM). Then, the correlation between the screening evaluation index and the multiple parameters was obtained, and the significant order of the parameters influencing the screening evaluation index was $F_t > f > n$.

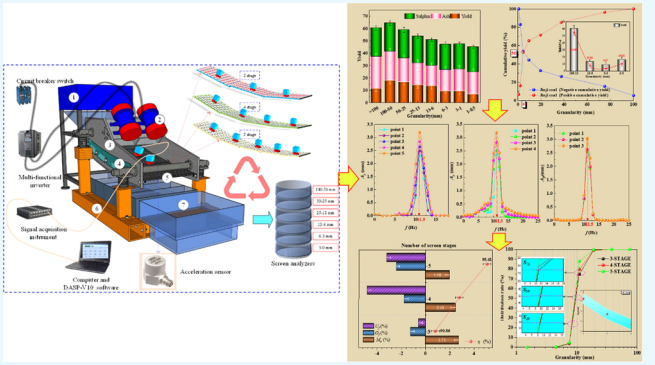

1. INTRODUCTION

Studies show that China has the largest proven reserve of coal in the world. China's coal reserves are estimated at more than 5.9 trillion tons. Coal reliably guarantees our life and economic development.[1−3] In 2020, the annual total energy consumption in China exceeded 4.98×10^9 tons of standard coal equivalent. In this regard, coal alone accounts for 56.8% of China's total energy consumption with an annual increase of 1.4%.[4−6] China's energy consumption structure is characterized by more coal, less oil, and poor gas. Thus, it is predicted that the role of coal as the main primary energy source will not change in the next few decades.[7−9] Coal resources have significantly contributed to the national economy while also causing serious environmental pollution. A low-degree clean utilization of coal and stagnation in the percentage of permission have seriously restricted the quality and the efficiency of the enterprise.[10−12]

Appropriate coal preparation is the most effective method to approach the clean coal concept.[2,13] The screening operation is a critical process of coal beneficiation, which is widely used in mineral classification, coal desliming, tailings dewatering, and product demineralization.[14−16] The traditional linear vibrating screens are easily accumulated at the feeding end when the production load increases. This problem makes it difficult for fine particles to penetrate the screen, so the screening effect cannot satisfy the normal needs of the enterprise.[17,18] To solve this problem of material accumulation, in the 1960s, Burstlein proposed an equal-thickness screening method on the basis of the models to simulate motions of material flocks. The main feature of this method is that the layer thickness on the screen remains unchanged during the screening process. Here, particles smaller than the screen aperture evenly permeate in the material flow so that the flow through the screen is stable.[19,20] On the basis of the variation method, Liu et al. applied Johann Bernoulli's fastest drop diameter problem to the development of the equal-thickness screen surface. They proposed a new screen surface applied to the infeed end, which could allow the finished material to be conveyed quickly. They also derived the curve equation and proposed a method for industrial application.[21]

Recently, the discrete element method (DEM) has been applied to simulate a double-decker banana screen for

Received: January 21, 2022
Accepted: April 6, 2022
Published: April 18, 2022

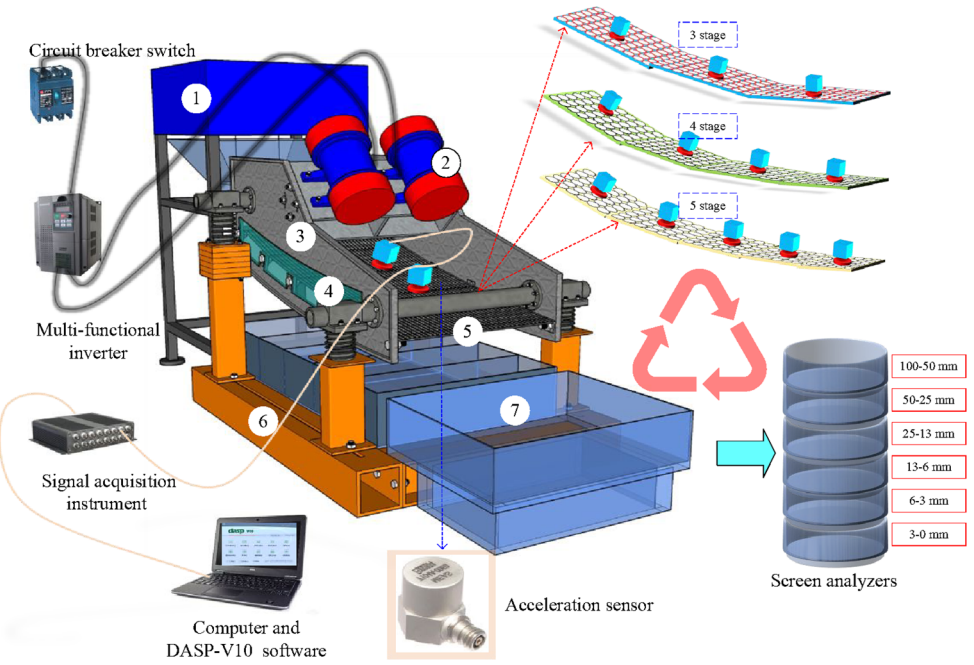

Figure 1. Schematic illustration of the multistage variable-inclination equal-thickness screen experiment and vibration test analysis system: 1, feeding devices; 2, excitation motors; 3, adjustable inclination angle side panel; 4, observation window; 5, screen surface; 6, supporting frame; 7, receiving devices.

industrial applications and analyzed the motion law of the material group on the screen under different acceleration conditions. It was pointed out that the critical issue associated with the design of double-decker banana screens is the rapid deep delamination on the bottom screen surface to play the role of the permeable screen. They also analyzed the particle yield of the material on and off the screen to conduct an overall evaluation of the screening performance.[22,23] Zhao et al. simulated the effects of the inclination of the screen surface and the aperture size on the separation size and the performance of the screening process on the basis of the DEM. They simulated the motion behavior and process of the material on the screen to investigate the kinetic characteristics of the particle population on the screen surface.[24,25] On the basis of the mechanical model of the banana screen, Asbjörnsson et al. proposed a modified configuration for the screen deck. The developed model could be used to optimize the screen surface for the realization of the optimal performance under different feed conditions to obtain the desired screening performance.[26] Fernandez et al. used the smoothed particle hydrodynamics (SPH) model and the DEM for the one-way coupling to study the screening performance of industrial banana screens used for moist materials. The screening efficiency and the distribution of flow velocity along the screen surface were obtained, and the SPH model was more accurate for the numerical simulation of wet particles with high flow velocities.[27] Jahani et al. used the self-developed LIGGHTS (an open-source software package) solver to simulate the screening process of double-deck and single-deck banana screens. It is worth noting that the former screen was in an industrial size while the latter one was a laboratory-scale one. They studied the variation of the screening efficiency under different conditions of the inclination, the amplitude, and the frequency to provide a parameter basis for the development of vibrating screens.[28] Huang et al. applied the high-speed dynamic analysis method to investigate variations of the displacement and the velocity of the screen surface motion. They provided the optimization scheme for different operation parameters based on the multiparameter response surface test method.[29] Dong et al. performed numerical simulations and applied the DEM to process banana screens with 3 and 5 stages. They explored the governing law of the particle motion and the screening effect such as the true toxicity, the frequency, the vibration mode, and the inclination angle of each stage and obtained the distribution law of the particle size composition for different materials.[30−32]

A review of the literature indicates that many investigations have been carried out on the screening performance of banana screens. In this regard, different structural parameters have been investigated by motion characteristics of the grain population on the screen surface. However, the time-frequency response characteristics of the multistage screen surface and the permeability pattern of the grain population have not yet been elucidated. Meanwhile, the impact of these parameters on the screening performance and the synergistic mechanism of these parameters are not clear yet.

In this work, a model of the collision mechanics between particles and the multistage variable-inclination screen surface was established. The time-frequency response characteristics of multistage (3-, 4-, and 5-STAGE) screen surfaces were studied by the vibration test analysis system. The distribution law of grain groups on the permeation screen surface was revealed by conducting screening experiments. The synergistic mechanism between two of the parameters (the excitation force, the excitation frequency, and the screen surface stages) was revealed. The correlation model between the screening evaluation index and multiple parameters was obtained, and the order of significance between two of the operational parameters was obtained by BBRSM (Box−Behnken response surface methodology). This research provided technical guidance for the optimal design of banana screens with industrial applications.

https://doi.org/10.1021/acsomega.2c00449
ACS Omega 2022, 7, 13963−13975

2. EXPERIMENTAL SECTION

2.1. Experimental Equipment. Figure 1 shows the experimental system for investigating the performance of a multistage variable-inclination equal-thickness screen. This system consisted of a control switch, a multifunctional inverter, a screen analyzer, a screen machine structure, and a vibration test analysis system. The structure of the screen machine was the basis for conducting the test, which consisted of feeding devices, an excitation motor, side plates, an observation window, a screen surface, a supporting frame, and receiving devices. A 0.6 m × 1.2 mm rigid perforated screen surface was used to classify materials by size and screen aperture.

During the experiment, the inclination angle and length of the screen surface remained constant, and the stage of the screen surface could be altered by an adjustable inclination device. During the vibration test, a signal acquisition instrument, a computer installed with the DASP-V10 software (software for data acquisition and waveform analysis, spectrum analysis and digital signal processing, and many other functions), and acceleration sensors, which were installed in the center of the different screen surfaces (3-, 4-, and 5-STAGE), were used. The role of the observation window was to follow the distribution regularities and the movement trajectory of the material group in real-time, and the support frame was used to adjust the inclination of the screen surface and fix the screen body. The main objective of the feeding devices was to store the material to be screened. Moreover, the feeder rate was adjusted using an inverter. Finally, oversized and undersized products were gathered using an appropriate receiving device. The screen analyzers were used to determine the particle size composition of the experimental results.

2.2. Vibration Test Analysis System. The operational procedure of the vibration test analysis system was as follows. First, the screen surface was evenly classified into several parts along the moving direction of the material. The measurement points were arranged in the middle of the screen surface and were attached to the magnetic seat by threads. The magnetic seat was vertically attached to the rigid screen surface by another strong magnetic seat as shown in Figure 1. The main technical specifications of the vibration testing analysis system are shown in Table 1.

Table 1. Key Technical Indexes of Vibration Testing and the Analysis System

number	operating parameters	indexes
1	measurement range	0−250 g
2	output signal range	≤8 V
3	operating voltage	+18 to +28 V (DC)
4	maximum working temperature	120 °C
5	output method	*x*, *y*, *z* three-way L5
6	resolution	1 mV (P−P)
7	total harmonic distortion	−70 dB
8	AD precision	24 position Δ−Σ Chip

The ICP acceleration sensor was installed along the *x*-direction parallel to the material flow. It should be indicated that this sensor was perpendicular to the screen surface and the side plate along the *y*- and *z*-directions, respectively. It was connected to the multichannel collector (INV3060S, China, China Orient Institute of Noise & Vibration) by a shielded cable, while the collector was connected to the computer installed with the DASP-V10 software by a Gigabit network cable.

An insulating tape was used to secure the shielded cable so that the stretching of this cable did not affect the acceleration sensor. The speed of the excitation motor was set by the inverter and the start time was set to 10 s. The sampling parameters were set by the DASP-V10 software, and then, the experiment system was turned on for data acquisition.

Next, the experiment system for the signal acquisition and the vibrating screen were turned on simultaneously. When the screen machine was operating steadily, the signal acquisition was conducted for approximately 5 min. After that, the inverter and the circuit breaker were turned off, and we waited until the screen machine was completely stationary. Finally, the signal acquisition was stopped, and the data were saved.

To achieve a better description of the signal, the sampling frequency needed to meet the Nyquist sampling theorem; that is, the sampling frequency was larger than twice the highest frequency in the signal. Generally, the sampling could be taken 8−10 times. The acceleration signal was transmitted to the computer via the shielded cable, the multichannel data acquisition instrument, and the network cable, and then, the collected signal in the time and frequency domains and Lissajous were analyzed in the DASP-V10 software environment.

2.3. Material Properties and Evaluation Indexes. In the present study, coal samples were obtained from the Jinji mine. The standard screening analyzer was used to conduct large and small screening experiments to determine the composition of ash and particle in the prepared samples. Then, the sulfur content was measured. In this regard, Figure 2a indicates that the dominant grain classes of the Jinji coal accounting for 49.12% of the yield of the whole sample were 100−50, 50−25, and 25−13 mm. The dominant grain classes of the ash content were >100 mm and 100−50 mm accounting for 25.74% and 23.4%, respectively. The dominant grain classes of the sulfur content were 100−50 mm and 50−25 mm accounting for 23.12% and 22.83%, respectively. On the basis of the particle size composition of the coal samples shown in Figure 2a, the corresponding cumulative particle size curve could be plotted as shown in Figure 2b.

The yield of any granularity could be calculated on the basis of the diagram of the particle size. The corresponding yields for different particle sizes are shown in Table 2. It can be seen that the four different types of particle yield distribution were almost the same with the highest yield of 60.67% for fine particles and the lowest yield of 9.37% for hindrance particles.

The evaluation index of the screening performance included the screening efficiency, the total mismatch content, and the separation accuracy. Screening efficiency is defined as the total effective placement efficiency for coarse particles and fine particles; the total mismatch content is defined as the sum of the coarse particle mismatch content and the fine particle mismatch content. The separation accuracy, also known as the average probability deviation, is defined as the average of the particle size values corresponding to 75% of the distribution size curve and the corresponding particle size values corresponding to 25% of the distribution size curve. They can be calculated by the following eqs 1, 2, and 3, respectively.[29]

https://doi.org/10.1021/acsomega.2c00449
ACS Omega 2022, 7, 13963−13975

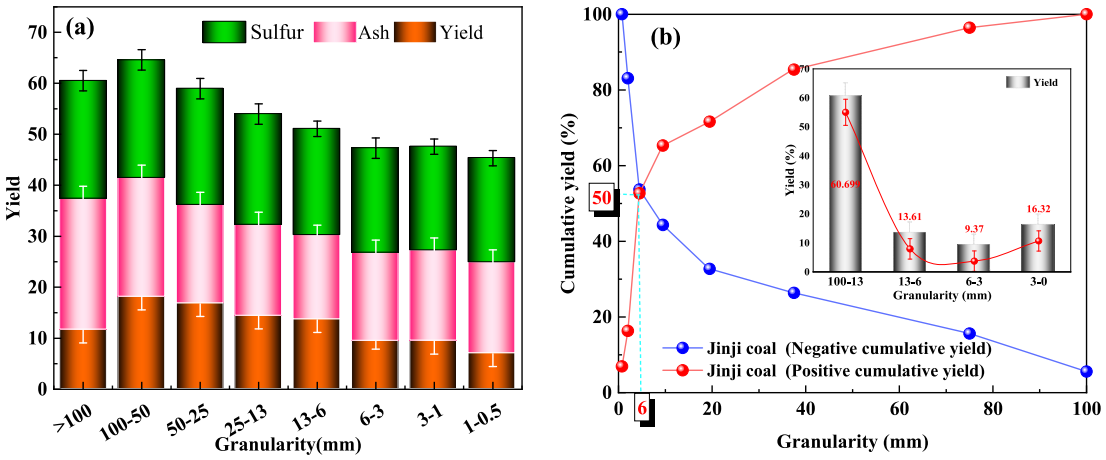

(a) Particle size composition (b) Corresponding cumulative particle size curve

Figure 2. Material properties of Jinji coal samples.

Table 2. Particle Types and Yields of Jinji Coal Samples

particle type	relative size/mm	particle size/mm	yield of Jinji coal/%
nonhindered particle	>1.50	100.00−13.00	60.669
hindrance particle	1.50−1.00	13.00−6.00	13.61
near-mesh particle	1.00−0.75	6.00−3.00	9.37
fine particle	<0.75	3.00−0.00	16.32

$$\begin{cases} \eta = E_c + E_f - 100 \\ E_c = \dfrac{\gamma_o \times O_c}{F_c} \times 100 \\ E_f = \dfrac{F_f - \gamma_o \times O_f}{F_f} \times 100 \end{cases} \quad (1)$$

$$\begin{cases} M_o = M_c + M_f \\ M_c = 100\gamma_u U_c \\ M_f = 100\gamma_o O_f \end{cases} \quad (2)$$

$$E_{pm} = \frac{S_{75} - S_{25}}{2} \quad (3)$$

where S_{75} and S_{25} denote the particle sizes corresponding to the distribution ratio of 75% and 25% on the distribution curve, respectively.

3. RESULTS AND DISCUSSION

3.1. Mechanical Model of Particle Collisions on a Multistage Variable-Inclination Screen Surface. The screening process is highly complex, with particles of different shapes and particle sizes mixed together and colliding with each other, making it difficult to analyze their movement patterns.[34] In order to study the particle collision separation mechanism and motion characteristics in the screen surface, the particle group and screen surface collision impact model are simplified to establish a single particle collision two-dimensional model with the screen surface.

The mechanics of the particle on the screen surface are modeled as shown in the Figure 3 with the displacement at any point on the screen surface.

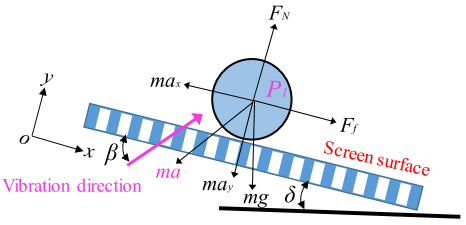

Figure 3. Two-dimensional mechanical model of single particle collision at the screen surface. The screen surface structure is composed of n stages of different inclination angles.

$$\begin{cases} x = A\cos\beta\sin\omega t \\ y = A\sin\beta\cos\omega t \end{cases} \quad (4)$$

where A is the amplitude of the screen surface in the direction of vibration, mm; β is the vibration direction angle, °; ω is the angular velocity, rad/s.

$$\begin{cases} F_f + m_p g\sin\delta = ma_x \\ F_N - m_p g\cos\delta = ma_y \end{cases} \quad (5)$$

With the x-direction along the screen surface and the y-direction perpendicular to the screen surface, an xoy coordinate system was established and the equilibrium equation for the forces on the screen surface for a single particle is

$$\begin{cases} F_f + m_p g\sin\delta + m_p A\omega^2\cos\beta\sin\omega t = 0 \\ F_N - m_p g\cos\delta + m_p A\omega^2\cos\beta\sin\omega t = 0 \end{cases} \quad (6)$$

where m_p is the mass of a single particle, kg; F_f is the frictional force on the screen surface on the particle, N; F_N is the pressure on the screen surface on the particle, N; g is the acceleration of gravity, m/s^2; δ is the angle of inclination of the screen surface, °.

The critical pressure at which the particle is thrown off the screen surface is regarded as $F_N = 0$, and the mechanical equilibrium equation can be simplified as

$$\sin\varphi = \frac{g\cos\delta}{A\omega^2\sin\beta} = \frac{\cos\delta}{k\sin\beta} = \frac{1}{K_v} \quad (7)$$

https://doi.org/10.1021/acsomega.2c00449
ACS Omega 2022, 7, 13963−13975

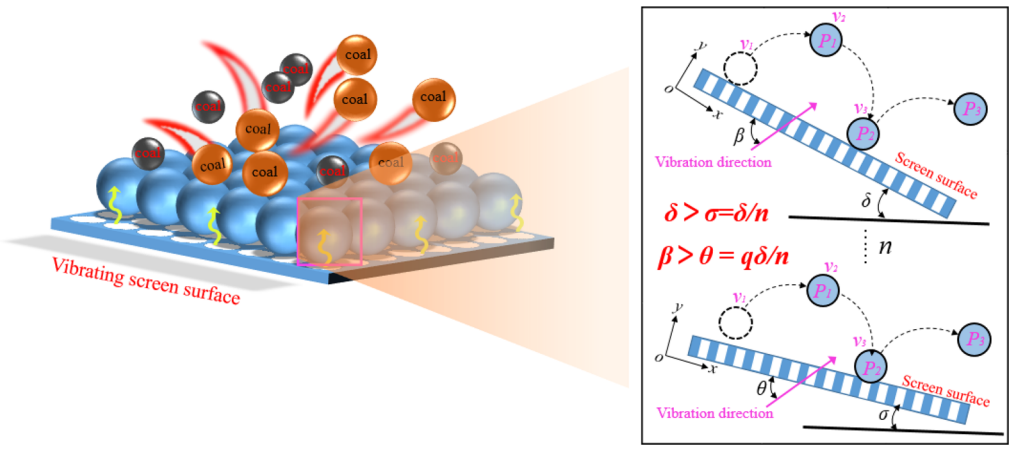

Figure 4. Particle movement on screen surfaces with different inclinations.

$$K_v = \frac{A\omega^2 \sin\beta}{g\cos\delta} \tag{8}$$

Figure 4 shows the motion of particles on the screen surface at different inclination angles. When the particles move on the nth stage screen surface, if the particles break away from the screen surface at time t_0 and do a projectile motion, the equation can be obtained.

$$A\omega^2 \sin\theta \sin\omega t_0 = g\cos\sigma \tag{9}$$

$$t_0 = \frac{1}{\omega}\text{acr}\sin\left(\frac{g\cos\sigma}{A\omega^2\sin\theta}\right) \tag{10}$$

The inclination angle of different screen surfaces is distributed in equal gradients; the vibration direction angle changes due to the change of the inclination angle of the screen surface, and the vibration direction and the horizontal angle are constant. Therefore, the vibration direction angle and the inclination angle of the screen surface can be obtained as a linear function.

$$\sigma = \frac{1}{n}\delta \tag{11}$$

$$\theta = \frac{q}{n}\delta \tag{12}$$

The starting velocity of the projection when the particle leaves the screen surface is v_1. After the particle leaves the screen surface, it is only subjected to gravity in the air, and the whole projectile motion ends when the particle touches the screen surface again; the time of the whole process is Δt_0.

$$\begin{cases} v_{1x} = A\omega\cos\theta\cos\omega t_0 \\ v_{1y} = A\omega\sin\theta\cos\omega t_0 \end{cases} \tag{13}$$

$$\Delta t_0 = \frac{2A\omega\sin\theta\cos\omega t_0}{g\cos\sigma} \tag{14}$$

When the particles touch the screen surface again, the velocity at which they collide with the surface is v_2. The particles collide with the screen surface at moment t_1. The collision force is perpendicular to the screen surface, and in the direction perpendicular to the screen surface, the external forces affecting the change in particle momentum are mainly the particle collision force and gravity, which can be obtained according to the momentum theorem.

$$\begin{cases} v_{2x} = A\omega\cos\theta\cos\omega t_0 + g\sin\sigma\Delta t_0 \\ v_{2y} = A\omega\sin\theta\cos\omega t_0 \end{cases} \tag{15}$$

$$m_p(v_{2y} + v_{3y}) = \int_{t_1}^{t_1+\Delta t_1} F(t)\,\mathrm{d}(t) - \int_{t_1}^{t_1+\Delta t_1} m_p g\cos\sigma\,\mathrm{d}(t) \tag{16}$$

$$v_{3y} = \lambda v_{2y} \tag{17}$$

$$\overline{F} = \frac{1}{k}F_{\max} \tag{18}$$

where v_{3y} is the bounce velocity of the particle in the vertical direction of the screen surface, m/s; $F(t)$ is the collision force between the particle and the screen surface as a function of time; Δt_1 is the time elapsed in the collision process, s; λ is the recovery coefficient normal to the screen surface, taking the value range $[0, 1]$; $\overline{F}$ is the average collision force between the particle and the screen surface in Δt_1 time, N; $F_{\max}$ is the maximum peak of the force in the collision process, N; k is the amplification factor of the collision force. Theoretically, the maximum collision force should be greater than the average collision force; k is a factor greater than 1.

The substitution of eqs 17 and 18 into eq 16 can introduce eq 19, and the $F_{\max}$ expression can be obtained by solving

$$\begin{aligned} m_p(v_{2y} + v_{3y}) &= \overline{F}\Delta t_1 - m_p g\cos\sigma\Delta t_1 \\ &= \Delta t_1\left[\frac{1}{k}F_{\max} - m_p g\cos\sigma\right] \end{aligned} \tag{19}$$

$$F_{\max} = k\left[\frac{m_p(v_{2y} + v_{3y})}{\Delta t_1} + m_p g\cos\sigma\right] \tag{20}$$

Yang and Guan obtained an ephemeral period during the collision of single particles by experimental methods.[33] Due to the fact that the study uses a rigid perforated screen surface, the deformation of the screen surface is small and ignored, and the height at which the particles are thrown up is H. The equation is simplified to obtain the collision period Δt_1.

$$H = \frac{v_{2y}^2}{2g} \tag{21}$$

https://doi.org/10.1021/acsomega.2c00449
ACS Omega 2022, 7, 13963−13975

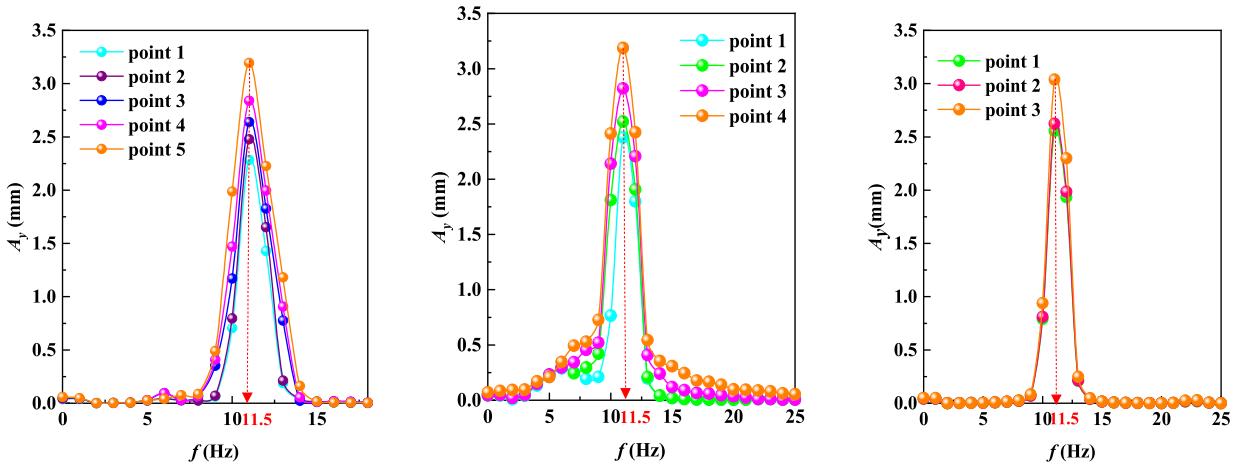

Figure 5. Frequency domain characteristic curve of each measuring point on the multistage screen surface in the process of equal-thickness screening.

$$\Delta t_1 = \frac{1}{100}\left(0.097 m_p g + \frac{0.09}{v_{2y}^{\ 2}} + 1.2\right) \tag{22}$$

When one substitutes eq 22 into eq 20, eq 23 is obtained. As the angular speed adjustment is achieved by changing the frequency of the inverter in the actual experiment, eq 23 will be collated.[34]

$$F_{max} = \left[\frac{100 m_p (v_{2y} + v_{3y})}{0.097 m_p g + \frac{0.09}{v_{2y}^{\ 2}} + 1.2} + m_p g \cos\sigma\right] \tag{23}$$

$$F_{max} = \frac{200(1+\lambda) k m_p A \pi f \sin\left(\frac{q\delta}{n}\right)\sqrt{1 - \left(\frac{g\cos\left(\frac{1}{n}\delta\right)}{4A\pi^2 f^2 \sin\left(\frac{q\delta}{n}\right)}\right)^2}}{0.097 m_p g + \frac{0.09}{4A^2\pi^2 f^2 \sin\left(\frac{q\delta}{n}\right)^2\sqrt{1 - \left(\frac{g\cos\left(\frac{1}{n}\delta\right)}{4A\pi^2 f^2 \sin\left(\frac{q\delta}{n}\right)}\right)^2}}} + k m_p g \cos\left(\frac{1}{n}\delta\right) \tag{24}$$

Equation 24 shows that the maximum collision force between the particles and the screen surface is related to the amplitude (A), frequency (f), inclination of the screen surface (δ), and the number of screen stages (n). When one adjusts the inclination of the screen surface and the number of stages, the collision force of the particles can be changed, thus enhancing the loosening and stratification effect of the material and enhancing the permeability of the screen.

3.2. Time-Frequency Response of Multistage Variable-Inclination Equal-Thickness Screening. As shown in Figures 4 and 5, when one uses the DASP-V10 software, the collected acceleration signals could be transformed into the time-domain and frequency-domain characteristic curves at each measuring point on the screen surface of multistage variable-inclination equal-thickness screening through the Fourier integral transform under the stable operation. Figure 5 indicates that the displacement waveforms in the y-axis direction of the measuring points on the screen surface (3-, 4-, and 5-STAGE) were close to the harmonic sine wave, and the dominant frequency of the screen surface was 11.5 Hz. The displacement amplitude of the measuring points on the screen surface (3-, 4-, and 5-STAGE) decreased gradually from the infeed to the outfeed ends.

Figure 6a reveals that the time-domain characteristic curve of the displacement amplitude along the y-axis of the measuring points on the 5-STAGE screen surface. Along the coal flow migration, the displacement amplitudes of the measuring points 1 and 5 in the y-axis direction were 2.4 and 3.1 mm, respectively. Accordingly, the difference of the displacement amplitude between the measuring points 1 and 5 was 0.7 mm, meaning that the amplitude difference ΔA between the screen surfaces of the stages V and I was 0.7 mm.

Figure 6b illustrates the time-domain characteristic curves of the displacement amplitude in the y-axis direction of the measuring points on the 4-STAGE screen surface. The displacement amplitudes of the measuring points 1 and 4 in the y-axis direction were 2.6 and 3.1 mm, respectively. The displacement amplitude difference between the measuring points 1 and 4 was 0.5 mm, meaning that the displacement amplitude difference ΔA between the screen surfaces of the stages IV and I was 0.5 mm.

Moreover, Figure 6c presents the time-domain characteristic curves of the displacement amplitude in the y-axis direction of the measuring points on the 3-STAGE screen surface. The displacement amplitudes of the measuring points 1 and 3 in the y-axis direction were 2.75 and 3.15 mm, respectively. The displacement amplitude difference between the measuring points 1 and 3 was 0.4 mm, meaning that the displacement amplitude difference ΔA between the screen surfaces of the stages III and I was 0.4 mm.

The difference of the displacement amplitudes between the measuring points on stages 1 and 5 of the 5-STAGE screen was the largest: it was the amplitude difference between the measuring points on the screen stages V and I. Then, the amplitude difference of the 4-STAGE screen surface followed and that of the 3-STAGE screen surface was the smallest. This means that the amplitude difference between the measuring points on the screen stages III and I was the smallest. The amplitude difference shows variations in the collision force at each stage of the screen surface. The amplitude of the collision force of the 5-STAGE of the screen was the largest and that of the 3-STAGE was the smallest. Each stage had a different inclination angle at the last stage of the screen surface, and the inclination angle of the last stage of the 5-STAGE was smaller than those of the 3-STAGE and the 4-STAGE. This resulted in

https://doi.org/10.1021/acsomega.2c00449
ACS Omega 2022, 7, 13963−13975

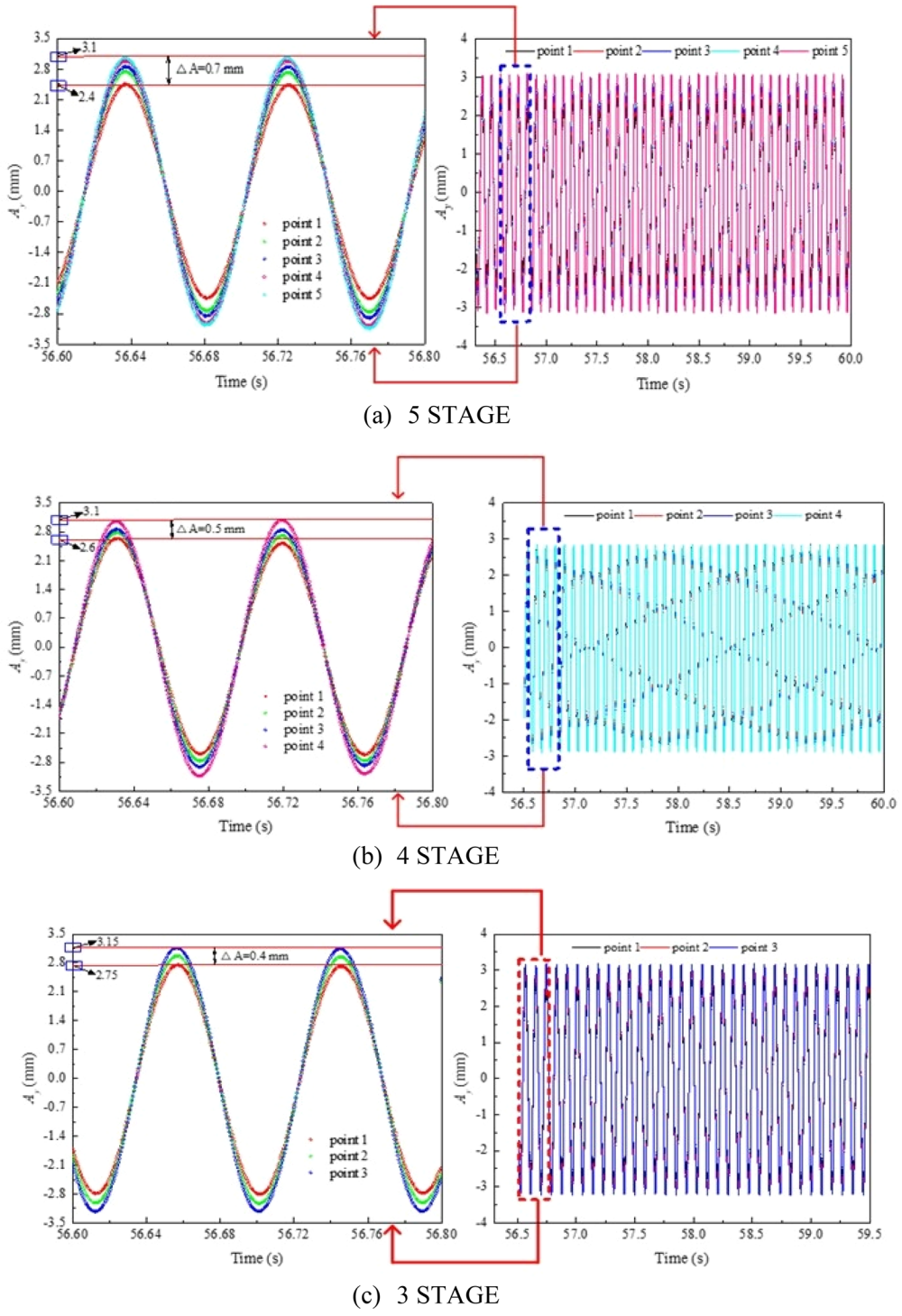

Figure 6. Time domain characteristic curve of each measuring point on the multistage screen surface in the process of equal-thickness screening.

a higher amplitude of the collision force of the 5-STAGE screen surface than those of other screens. The amplitude of the collision force has a direct impact on the loose movement of coal samples and the effect of penetration and stratification. Our experimental results verified the reason the 5-STAGE screen surface has been widely used in the classification operation stage.

Figure 7 shows variation curves of the displacement, acceleration, and velocity of the measuring points along the *y*-axis in different areas. The displacement, acceleration, and velocity of each measuring point along the *y*-axis direction gradually decreased, and their intercepts and slopes on the *y*-coordinate axis were all positive. It can be seen that the mathematical models expressing the relationship between the physical parameters (the velocity, displacement, and acceleration) and the number of stages for the measuring points along the *y*-axis were obtained by the linear regression analysis. The mathematical models were in the linear form of $y = bx + a$; that is, the physical parameters in the *y*-axis direction of the screen surface were linearly related to the number of stages on the screen surface.

https://doi.org/10.1021/acsomega.2c00449
ACS Omega 2022, 7, 13963−13975

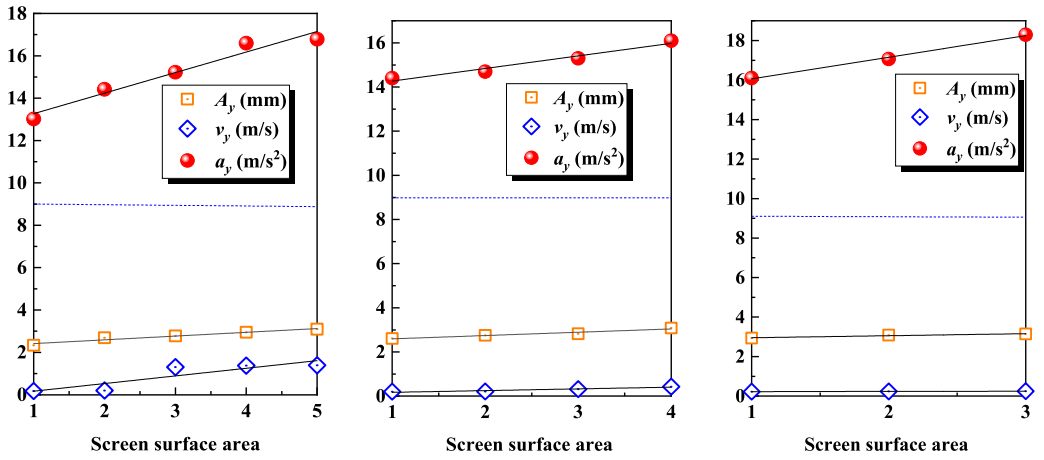

Figure 7. Variation curve of displacement, acceleration, and velocity of each measuring point in the *y*-axis direction in different areas of the screen surface.

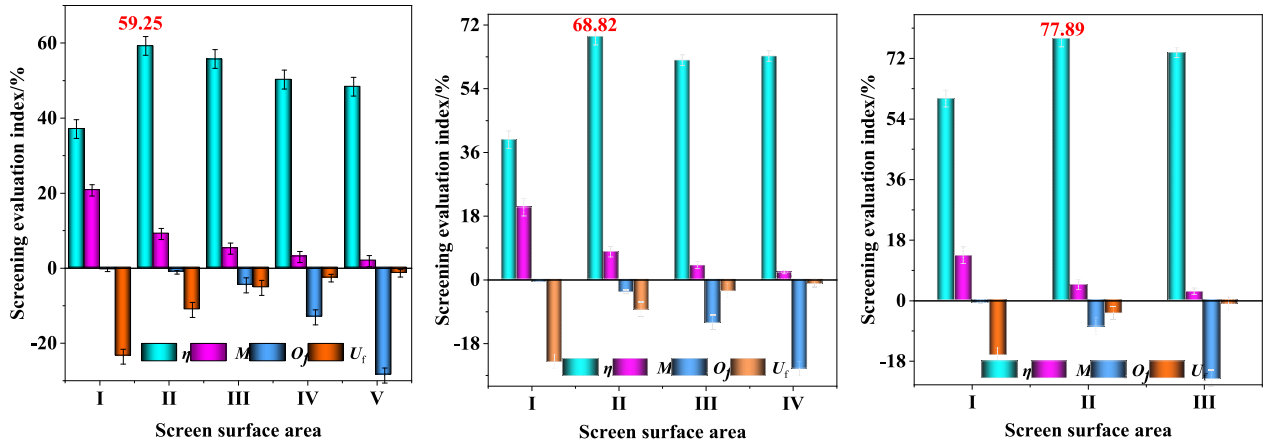

Figure 8. Curves of the screening index under different screen surface stages.

3.3. Effect of the Screen Surface Stages on the Distribution Pattern of Permeable Screens and the Screening Performance of Particle Groups. In this research, the variation of the screen stages was mainly realized by the adjustment device with the special inclination angle. During the experiment, the excitation combined force was adjusted to 8.66 kN. The excitation frequency was 11.84 Hz; the production capacity was 10.8 t/h, and the feeding time was 10 s. The above conditions were kept throughout the experiments, and the screen length was constant. For the 6 mm screening experiment, the 3-, 4-, and 5-STAGE screen surfaces were selected and the multistage sampling analysis was conducted. The 6-STAGE screen surface was not selected; it is used for desliming and dewatering, which are not in the scope of this study. The experimental results are shown in Figures 8 and 9.

Figure 8 illustrates the screening index under different screen surface stages. It is observed that the variation trend of the screening efficiency, the total mismatch content, the oversize fraction, and the undersize fraction on the screen surface of each stage was the same. The screening efficiency of each stage increased first and then decreased, while the total mismatch content decreased gradually. The oversize fraction increased gradually, while the undersized fraction decreased gradually. The obtained results revealed that the best screening performance was achieved in the second stage of the screen surface. The screening efficiency of the third, fourth, and fifth stages reached the maximum values of 59.25%, 68.82%, and 77.89%, respectively. This indicates that the samples were centrally penetrating in the middle of the screen surface and the second stage area had the largest amount of screening. The stage of the screen surface did not affect the position of the coal samples.

The variation curves of the particle size distribution and the separation accuracy under different screen stage conditions are shown in Figure 9. All the distribution curves of the screen surfaces (3-, 4-, and 5-STAGE) moved to the right, and all the distribution curves of the particle sizes S_{25}, S_{50}, and S_{75} increased first and then decreased. All the E_{pm} values decreased first and then increased. For the 5-STAGE screen surface, the maximum and minimum values of S_{50} were 5.28 and 2.76 mm, respectively, and the maximum and minimum values of E_{pm} were 2.45 and 1.05 mm, respectively. For the 4-STAGE screen surface, the maximum and minimum values of S_{50} were 5.25 and 4.61 mm, respectively, and the maximum and minimum values of E_{pm} were 2.065 and 1.355 mm, respectively. For the 3-STAGE screen surface, the maximum and minimum values of S_{50} were 5.54 and 4.25 mm, respectively, and the maximum and minimum values of E_{pm} were 1.995 and 0.965 mm, respectively. Both S_{50} and E_{pm} reached the highest values in the second stage of the screen surface.

https://doi.org/10.1021/acsomega.2c00449
ACS Omega 2022, 7, 13963−13975

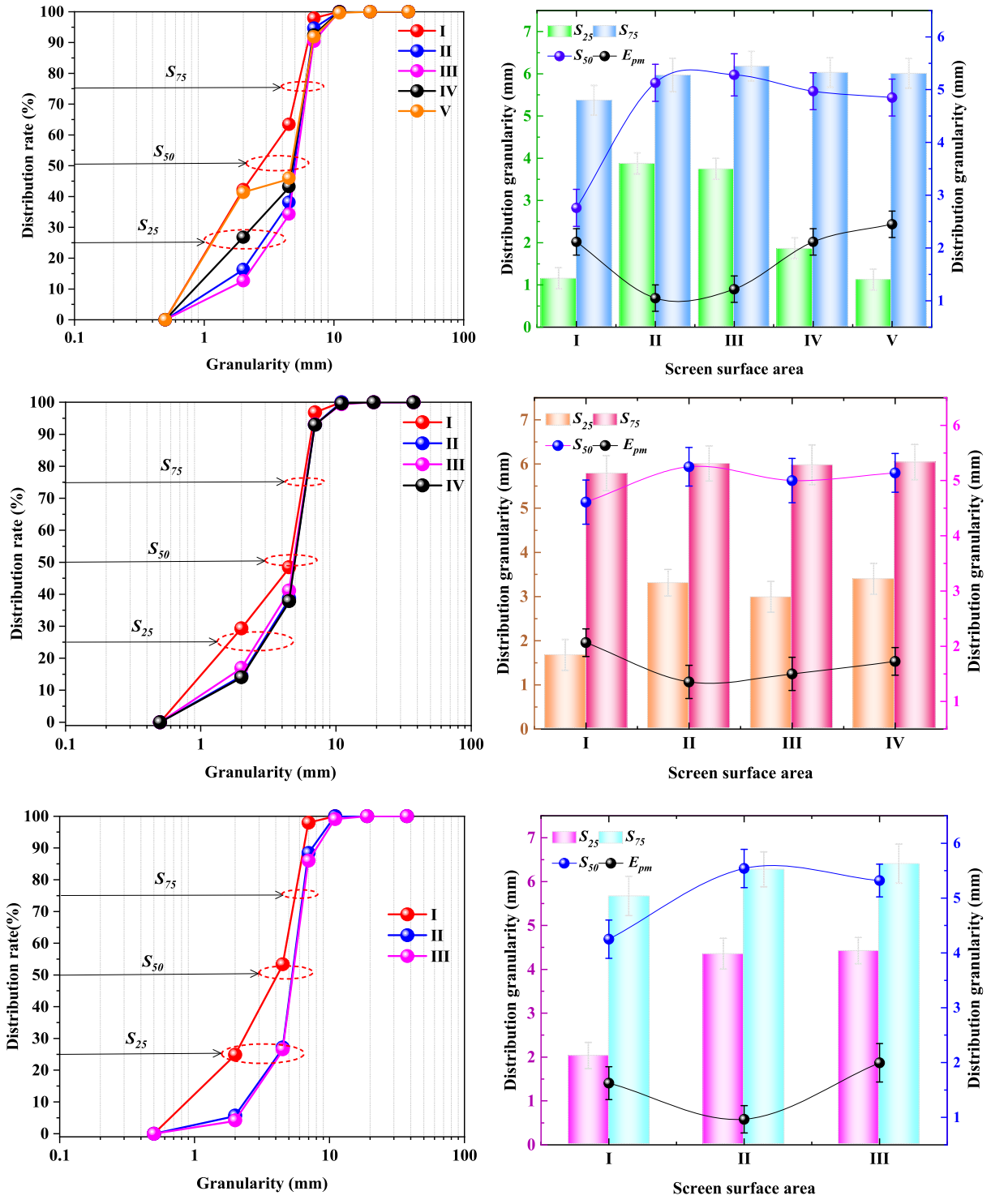

Figure 9. Curves of distribution particle size and separation accuracy under different screen surface stages.

Figure 10 illustrates the influence of the screen surface stages on the evaluation index of the screening performance. With the increase of the screen stage, the distribution curve moved to the left and the particle size distribution curve gradually, up to the left. The particle size and the separation accuracy of the 4-STAGE screen surface were the smallest, followed by the 3-STAGE screen surface, and the highest was the 5-STAGE screen surface. It can be seen that the variation of different stages of the screen surface had an undeniable impact on the screening efficiency and the total mismatch content. With the increase in the stages, the screening efficiency gradually increased, while the total mismatch content gradually decreased. In this regard, the highest screening efficiency was 95.61%, which was achieved for the 5-STAGE screen surface, and the second highest was for the 4-STAGE, while the smallest was for the 3-STAGE.

3.4. Parameter Co-optimization of the Multistage Variable-Inclination Equal-Thickness Screen (MSVIETS) Using the Box-Behnken Response Surface Method (BBRSM). In this study, it was found that the experimental

https://doi.org/10.1021/acsomega.2c00449
ACS Omega 2022, 7, 13963−13975

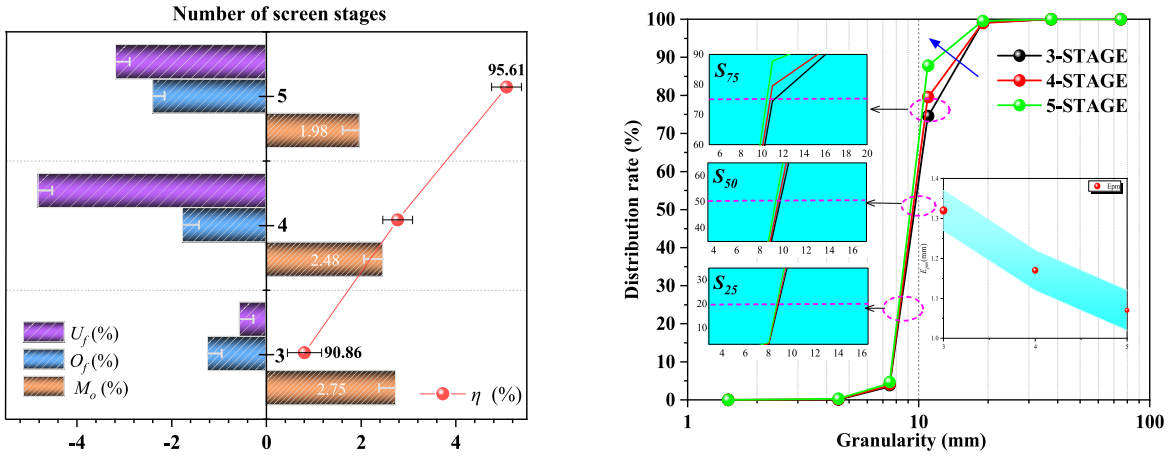

Figure 10. Trend diagram of the influence of the number of screen stages on the evaluation index of the screening performance.

parameters, such as the excitation frequency (f), the number of screen surface stages (n), and the excitation combined force (F_t) significantly affected the screening performance. Also, further evaluation of the significance and the interaction of these parameters using BBRSM is required to obtain the optimum conditions.

Experimental results of the VAETES are shown in Table 3. Table 3 lists the investigated factors, and their levels were selected on the basis of the experimental results of single-factor screening experiments. There were three factors including the excitation force, excitation frequency, and the number of screen stages, each of which had three distinct levels. The average value of each factor was the best level in the single-factor experiments. Their corresponding minimum and maximum values were at the same level as the selected optimal values. A total of 17 experiments were designed using BBRSM. The screening performance was evaluated using screening efficiency and total mismatch content.

Table 4 shows the estimation of the coefficients of screening efficiency, total mismatch content, and each factor. The coefficients estimate the model according to BBRSM, where the intercept coefficient was the intercept, i.e., the constant term, and since the estimated values of the coefficients A, B, C, AB, AC, and BC were known, a quadratic response prediction model between screening efficiency, total mismatch content, and each factor could be obtained, as shown in eqs 25 and 26. This indicates that the experimental results were very reliable and well-predicted as well as that the quadratic model could be used to navigate the design space.

Table 3. Experimental Results of the BBRSM Screening Experiment

experiment no.	F_t (kN)	f (Hz)	n (block)	η (%)	M (%)
1	8	36	3	89.77	2.98
2	8	40	1	86.89	4.02
3	9	32	3	85.16	4.22
4	7	32	3	92.38	2.36
5	7	40	3	90.05	2.78
6	8	36	3	89.77	2.98
7	7	36	5	94.36	2.03
8	8	36	3	89.77	2.98
9	8	32	5	89.61	3.08
10	7	36	1	89.19	3.17
11	9	36	1	88.69	3.44
12	9	36	5	87.42	3.82
13	8	40	5	90.27	2.81
14	8	36	3	89.77	2.98
15	9	40	3	87.65	3.69
16	8	36	3	89.27	3.04
17	8	32	1	88.54	3.53

Table 4. Estimation of Coefficients for Each Factor of the Prediction Model for Screening Efficiency and Total Mismatch Content

	coefficient estimation	
factor	η	M_o
intercept	89.67	2.99
$A-F_t$	−2.13	0.6038
$B-f$	−0.1037	0.0138
$C-n$	1.04	−0.3025
AB	1.20	−0.2375
AC	−1.61	0.3800
BC	0.5775	−0.1900
A^2	0.1137	0.0127
B^2	−0.9738	0.2577
C^2	0.1313	0.1103

$$\eta = 89.67 - 2.13 \times F_t - 1.037 \times f + 1.04 \times n + 1.20 \times F_t \times f - 1.61 \times F_t \times n + 0.578 \times f \times n + 0.114 \times F_t^2 - 0.9738 \times f^2 + 0.131 \times n^2 \quad (25)$$

$$M_o = 2.99 + 0.6034 \times F_t + 0.138 \times f - 0.303 \times n - 0.238 \times F_t \times f + 0.38 \times F_t \times n - 0.19 \times f \times n + 0.127 \times F_t^2 + 0.258 \times f^2 + 0.11 \times n^2 \quad (26)$$

Figure 11 shows the distribution of the screening efficiency and the total mismatch content for different operating parameters. It should be noted that the highest point on the response surface corresponds to the maximum value of the screening performance. Consequently, the corresponding parameters indicate the optimum operating conditions. In this regard, Figure 11a−c illustrates the screening efficiency response planes for F_t and f, f and n, and n and F_t combinations, respectively. Furthermore, Figure 11d,e shows

https://doi.org/10.1021/acsomega.2c00449
ACS Omega 2022, 7, 13963−13975

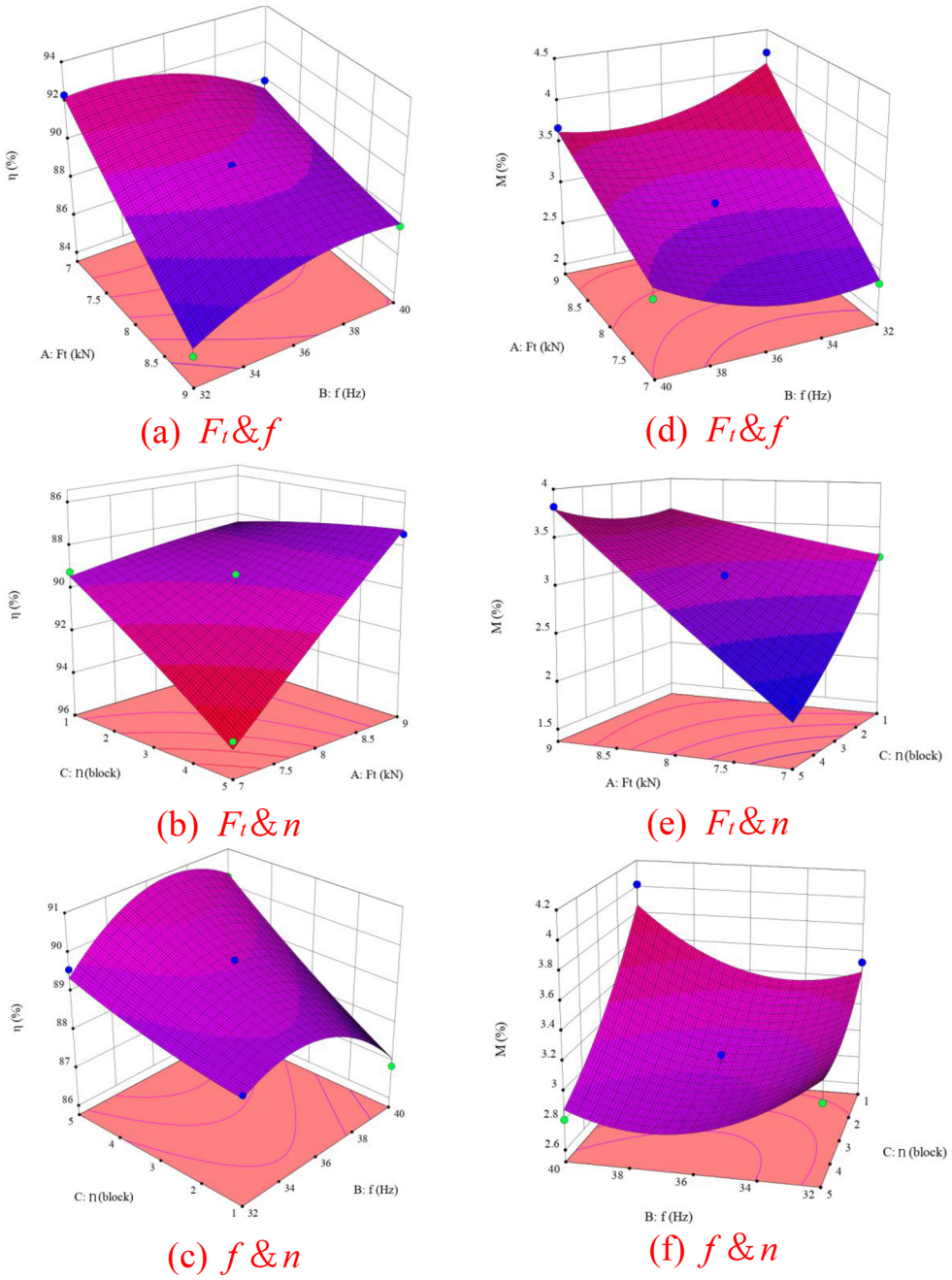

Figure 11. Response surfaces of η and M of MSVIETS under different combinations of the operating factors.

the response planes of the total mismatch content for the F_t and f, n and f, and F_t and n combinations, respectively.

Compared to parameter f, variations of F_t have a greater impact on the screening efficiency and the total mismatch content. That is, the smaller the change in F_t, the greater is the change in the screening performance (Figure 11a,d). The response shape along F_t was steeper than along n (Figure 11b,e). Moreover, the response shape was steeper along f than along n (Figure 11c,f). It should be indicated that the steeper the response shape, the higher is the effect on the screening efficiency. Thus, the order of the parameters with the greatest impact on η and M_o was $F_t > f > n$. The value of F_t had a more significant effect on the screening performance compared to the other two parameters.

4. CONCLUSION

In this research, the following conclusions were obtained. First, a model of the collision mechanics between the particles and multistage variable-inclination screen surface was established, and the maximum collision force (F_{max}) was found to be closely related to amplitude, frequency, screen surface inclination, and the number of stages. The displacement waveforms in the y-direction of the measuring points on the screen surface (3-, 4-, and 5-STAGE) were close to the harmonic sine wave, and the dominant frequency of the screen surface was 11.5 Hz. The displacement amplitude of the measuring points on the screen surface (3-, 4-, and 5-STAGE) decreased gradually from the infeed to outfeed ends, and the amplitude of the collision force of the 5-STAGE screen surface was higher than those of other screens. The physical

https://doi.org/10.1021/acsomega.2c00449
ACS Omega 2022, 7, 13963−13975

parameters in the y-axis direction of the screen surface were linearly related to the screen surface stages.

Second, the coal samples were centrally penetrating in the middle of the screen surface, and the second stage area had the largest amount of screening. The stage of the screen surface did not affect the location of the permeable screen. As the stage of the screen surface increased, the screening efficiency gradually increased and the total mismatch content gradually decreased. The highest screening efficiency was 95.61% for the 5-STAGE screen surface; the second highest was for the 4-STAGE screen surface, and the smallest was for the 3-STAGE screen surface. This verified the reason the 5-STAGE screen surface has been widely used in the classification operation stage.

Finally, the significant order of the parameters influencing η and M_o was $F_t > f > n$. We observed significant interactions between any of the two pairs of these parameters as well as their effects on the screening performance. The mathematical model expressing the relationship between η and M_o and the operating parameters was established by the regression analysis.

AUTHOR INFORMATION

Corresponding Authors

Haishen Jiang − *School of Chemical Engineering and Technology, Key Laboratory of Coal Processing and Efficient Utilization of Ministry of Education, China University of Mining & Technology, Xuzhou, Jiangsu 221116, China*; Email: haishen_jiang2015@163.com

Long Huang − *School of Chemical Engineering and Technology, Key Laboratory of Coal Processing and Efficient Utilization of Ministry of Education, China University of Mining & Technology, Xuzhou, Jiangsu 221116, China*; orcid.org/0000-0002-7407-9036; Email: hlong@126.com

Authors

Yuhan Liu − *School of Chemical Engineering and Technology, Key Laboratory of Coal Processing and Efficient Utilization of Ministry of Education, China University of Mining & Technology, Xuzhou, Jiangsu 221116, China*

Jiawang Lu − *School of Chemical Engineering and Technology, Key Laboratory of Coal Processing and Efficient Utilization of Ministry of Education, China University of Mining & Technology, Xuzhou, Jiangsu 221116, China*

Shijie Yu − *School of Chemical Engineering and Technology, Key Laboratory of Coal Processing and Efficient Utilization of Ministry of Education, China University of Mining & Technology, Xuzhou, Jiangsu 221116, China*

Miao Pan − *School of Chemical Engineering and Technology, Key Laboratory of Coal Processing and Efficient Utilization of Ministry of Education, China University of Mining & Technology, Xuzhou, Jiangsu 221116, China*

Jida Wu − *School of Agricultural Engineering and Food Science, Shandong University of Technology, Zibo 255000, China*

Jinpeng Qiao − *School of Chemical Engineering and Technology, Key Laboratory of Coal Processing and Efficient Utilization of Ministry of Education, China University of Mining & Technology, Xuzhou, Jiangsu 221116, China*

Complete contact information is available at: https://pubs.acs.org/10.1021/acsomega.2c00449

Notes

The authors declare no competing financial interest.

ACKNOWLEDGMENTS

This study is financially supported by the National Natural Science Foundation of China (52125403, 51904301, U1903132), the China Postdoctoral Science Foundation (2020M671652), the Science and Technology Project of Xuzhou City (KC21291), and Shandong modern agricultural industry technology system-corn industry innovation team construction project (SDAIT-02-12).

NOMENCLATURE

η	screening efficiency
E_c	effective placement efficiency of coarse particles
E_f	effective placement efficiency of fine particles
O_f	ratio of fine particles in the oversized product
O_c	ratio of coarse particles in the oversized product
U_c	ratio of coarse particles in the undersized product
M_o	total mismatch content
M_c	misplaced materials of coarse particles
M_f	misplaced materials of fine particles
γ_o	yield of the oversized product
γ_u	yield of the undersized product
F_c	ratio of coarse particles in the feeding
F_f	ratio of fine particles in the feeding
E_{pm}	separation accuracy

REFERENCES

(1) Chen, Z.; Huang, L.; Jiang, H.; Zhao, Y.; Liu, C.; Duan, C.; Zhang, B.; Yang, G.; Chai, J.; Ban, H.; Yu, S.; Wu, J. Application of screening using a flip-flow screen and shallow groove dense-medium separation in a steam coal preparation plant. *International Journal of Coal Preparation and Utilization* **2020**, 1.

(2) Jiang, H.; Wen, P.; Luo, Z.; Duan, C.; Zhao, Y.; Zhou, Z.; He, J.; Liu, C.; Wang, Z. Optimization of the disequilibrium excitation rigid-flex elastic screening process and its application for coal beneficiation. *International Journal of Coal Preparation and Utilization* **2020**, 1.

(3) Dong, L.; Zhu, F.; Li, Y.; Zhao, Y.; Duan, C.; Ren, Y.; Wang, G.; He, J.; Zhang, Y. Experimental and numerical study of the characteristics of the forced oscillation in a pulsation fluidized bed (PFB) for coal separation. *Chem. Eng. Sci.* **2021**, *234*, 116459.

(4) Dai, G.; Han, J.; Duan, C.; Tang, L.; Peng, Y.; Chen, Y.; Jiang, H.; Zhu, Z. Enhanced flotation efficiency of metal from waste printed circuit boards modified by alkaline immersion. *Waste Management.* **2021**, *120*, 795−804.

(5) Yu, X. D.; Li, H. B.; Luo, Z. F. Study on the effect of autogenous medium characteristics on oil shale beneficiation in the compound autogenous medium dry cleaning apparatus. *Fuel* **2021**, *287*, 119519.

(6) Jiang, H.; Yu, S.; Huang, L.; Zhao, Y.; Duan, C.; Wang, Q.; Luo, Z.; Liu, C.; Zhou, Z.; He, J.; Tang, L.; Cao, X. Kinematics and mechanism of rigid-flex elastic screening for moist coal under disequilibrium excitation. *International Journal of Coal Preparation and Utilization* **2020**, 1.

(7) Han, J.; Duan, C.; Lu, Q.; Jiang, H.; Fan, X.; Wen, P.; Ju, Y. Improvement of the crushing effect of waste printed circuit boards by co-heating swelling with organic solvent. *Journal of Cleaner Production.* **2019**, *214*, 70−78.

(8) Yao, Y.; Zhou, K.; He, J.; Zhu, L.; Zhao, Y.; Bai, Q. Efficient recovery of valuable metals in the disposal of waste printed circuit boards via reverse flotation. *Journal of Cleaner Production* **2021**, *284*, 124805.

(9) Zhu, L.; Zhang, M.; He, J.; Liu, C.; Yao, Y.; Xu, J.; Liu, B.; Yin, S.; Xu, X. Recovery of metal fractions from waste printed circuit boards via the vibrated gas-solid fluidized bed. *Advanced Powder Technology.* **2021**, *32* (2), 370−377.

(10) He, J.; Yang, J.; Tariq, S. M.; Duan, C.; Zhao, Y. Comparative investigation on copper leaching efficiency from waste mobile phones using various types of ionic liquids. *Journal of Cleaner Production* **2020**, *256*, 120368.
(11) Wen, P.; Duan, C.; Tang, L.; Qiao, J.; Jiang, H.; Wu, J. Study on noise characteristics of a novel equal-thickness screen. *Noise Control Engineering Journal.* **2020**, *68* (2), 168−178.
(12) Wu, J.; Liu, C.; Jiang, H.; Zhang, B. A vibration-test-based calculation method of screening material mass of a mining crank-link type flip-flow screen. *Energy Sources Part a-Recovery Utilization and Environmental Effects* **2020**, 1.
(13) Duan, C.; Zhou, C.; Dong, L.; Zhao, Y.; Liu, Q. A novel dry beneficiation technology for pyrite recovery from high sulfur gangue. *Journal of Cleaner Production.* **2018**, *172*, 2475−2484.
(14) Peng, L. P.; Feng, H. H.; Wang, Z. Q.; Wang, H. Y.; Yang, H.; Huang, H. Screening Mechanism and Properties of a Cantilevered Vibrating Sieve for Particles Processing. *Applied Sciences-Basel.* **2019**, *9* (22), 4911.
(15) Wang, Z.; Liu, C.; Wu, J.; Jiang, H.; Zhao, Y. Impact of screening coals on screen surface and multi-index optimization for coal cleaning production. *Journal of Cleaner Production.* **2018**, *187*, 562−575.
(16) Zhou, Z.; Huang, L.; Jiang, H.; Wen, P.; Zhao, L.; Zhao, Y.; Duan, C.; Luo, Z.; Wang, Z.; Liu, C.; Wang, Z. Kinematics of elastic screen surface and elimination mechanism of plugging during dry deep screening of moist coal. *Powder Technology* **2019**, *346*, 452−461.
(17) Wang, Z.; Liu, C.; Wu, J.; Jiang, H.; Song, B.; Zhao, Y. A novel high-strength large vibrating screen with duplex statically indeterminate mesh beam structure. *Journal of Vibroengineering.* **2017**, *19* (8), 5719−5734.
(18) Jiang, H.; Zhao, Y.; Duan, C.; Liu, C.; Wu, J.; Diao, H.; Lv, P.; Qiao, J. Dynamic characteristics of an equal-thickness screen with a variable amplitude and screening analysis. *Powder Technology.* **2017**, *311*, 239−246.
(19) Jiang, H.; Wang, W.; Zhou, Z.; Jun, H.; Wen, P.; Zhao, Y.; Duan, C.; Zhao, L.; Luo, Z.; Liu, C. Simultaneous multiple parameter optimization of variable-amplitude equal-thickness elastic screening of moist coal. *Powder Technology.* **2019**, *346*, 217−227.
(20) Jiang, H.; Zhao, Y.; Duan, C.; Yang, X.; Liu, C.; Wu, J.; Qiao, J.; Diao, H. Kinematics of variable-amplitude screen and analysis of particle behavior during the process of coal screening. *Powder Technology.* **2017**, *306*, 88−95.
(21) Liu, C.-s.; Zhang, S.-m.; Zhou, H.-p.; Li, J.; Xia, Y.-f.; Peng, L.-p.; Wang, H. Dynamic analysis and simulation of four-axis forced synchronizing banana vibrating screen of variable linear trajectory. *Journal of Central South University.* **2012**, *19* (6), 1530−1536.
(22) Cleary, P. W.; Sinnott, M. D.; Morrison, R. D. Separation performance of double deck banana screens - Part 1: Flow and separation for different accelerations. *Minerals Engineering.* **2009**, *22* (14), 1218−1229.
(23) Cleary, P. W.; Sinnott, M. D.; Morrison, R. D. Separation performance of double deck banana screens - Part 2: Quantitative predictions. *Minerals Engineering.* **2009**, *22* (14), 1230−1244.
(24) Zhao, L.; Zhao, Y.; Bao, C.; Hou, Q.; Yu, A. Optimisation of a circularly vibrating screen based on DEM simulation and Taguchi orthogonal experimental design. *Powder Technology.* **2017**, *310*, 307−317.
(25) Zhao, L.; Zhao, Y.; Sao, C.; Hou, Q.; Yu, A. Laboratory-scale validation of a DEM model of screening processes with circular vibration. *Powder Technology* **2016**, *303*, 269−277.
(26) Asbjörnsson, G.; Bengtsson, M.; Hulthen, E.; Evertsson, M. Model of banana screen for robust performance. *Minerals Engineering.* **2016**, *91*, 66−73.
(27) Fernandez, J. W.; Cleary, P. W.; Sinnott, M. D.; Morrison, R. D. Using SPH one-way coupled to DEM to model wet industrial banana screens. *Minerals Engineering.* **2011**, *24* (8), 741−753.
(28) Jahani, M.; Farzanegan, A.; Noaparast, M. Investigation of screening performance of banana screens using LIGGGHTS DEM solver. *Powder Technology.* **2015**, *283*, 32−47.
(29) Huang, L.; Pan, M.; Jiang, H.; Dong, L.; Duan, C.; Zhao, Y.; Qiao, J.; Yu, S.; Wang, Y. Kinematic characteristics of banana screen surface and operational parameter optimization for coal classification. *International Journal of Coal Preparation and Utilization* **2020**, 1.
(30) Dong, K. J.; Wang, B.; Yu, A. B. Modeling of Particle Flow and Sieving Behavior on a Vibrating Screen: From Discrete Particle Simulation to Process Performance Prediction. *Ind. Eng. Chem. Res.* **2013**, *52* (33), 11333−11343.
(31) Dong, K. J.; Yu, A. B. Numerical simulation of the particle flow and sieving behaviour on sieve bend/low head screen combination. *Minerals Engineering* **2012**, *31*, 2−9.
(32) Dong, K. J.; Yu, A. B.; Brake, I. DEM simulation of particle flow on a multi-deck banana screen. *Minerals Engineering.* **2009**, *22* (11), 910−920.
(33) Yang, Q.; Guan, B. Experimental study of methods for calculating the impact force of falling rocks. *Journal of Railway* **1996**, *18* (1), 101−106.
(34) Wang, Z.; Liu, C.; Wu, J.; Jiang, H.; Zhao, Y. Impact of screening coals on screen surface and multi-index optimization for coal cleaning production. *Journal of Cleaner Production.* **2018**, *187*, 562−575.

https://doi.org/10.1021/acsomega.2c00449
ACS Omega 2022, 7, 13963−13975